

FEDSM-ICNMM2010-1000

A COMPUTATIONAL MODEL FOR HYDRAULIC LABYRINTH SEALS

Rémi Boudierlique¹, François Guibault², André Garon³

École Polytechnique de Montréal

^{1,3}Department of Mechanical Engineering,

²Department of Computer Engineering and Software Engineering,
CP 6079, succ. Centre-Ville,
Montréal, Québec, H3C 3A7
Canada

Email: remi.boudierlique@polymtl.ca,
francois.guibault@polymtl.ca, andre.garon@polymtl.ca

Thi Vu

Andritz Hydro Ltd.

6100, TransCanadian highway
Pointe-Claire, Québec, H9R 1B9
Canada

Email: thi.vu@andritz-hydro.com

ABSTRACT

Every Francis turbine has a thin gap between rotating and non-rotating parts, which prevents contact between the two units. Although necessary, hydraulic seals create energetic losses: some fluid does not flow through the runner (leakage loss) and exerts a torque on the rotor (friction loss).

Only analytical and empirical prediction methods of a seal efficiency had been developed before 1980. Numerical methods are now used to predict seals performance. However, most of the studies known to the authors deal with gas labyrinth seals and use the $k - \epsilon$ turbulence model. In hydraulic seals, since the viscous losses in the boundary layer influence the leakage loss, low Reynolds turbulence models appear more appropriate. Our study aims to implement an accurate model to predict losses in labyrinth seals using a low Reynolds model, and validate it using experimental results. The issues of the mesh and boundary conditions are addressed. The commercial code ANSYS CFX 12 is used.

INTRODUCTION

In every Francis turbine, there is a thin gap between the rotating and stationary part of the runner. This gap, or hydraulic seal, prevents contact between the rotor and the stator, at the cost

of a small leakage flow that does not contribute to the turbine power extraction process. In the course of designing a hydraulic turbine, engineers seek to minimize the amount of leakage flow, while respecting geometric constraints such that no cavitation nor cold welding occur. Although necessary, hydraulic seals create energetic losses, a leakage loss and a frictional loss : the fluid flowing through the seal doesn't go through the turbine (leakage) and exerts a torque on the rotor (friction). To improve the seal energetic efficiency, a tortuous and highly frictional flow path is interposed between high and low-pressure regions. Three main types of geometries are widely used and studied in the literature : annular seals (also called straight through seals), straight through or stepped labyrinth seals, and stepped seals. Those geometries are represented on Fig. 1. Only analytical and empirical prediction methods of a seal efficiency had been developed before 1980 [1–7]. For example, experiences were lead by Andritz Hydro (formerly Dominion Engineering Works) in the sixties and seventies [4–8] constitute a major information source of our study. In particular, the tests reported in [4] are critical for our study: they are the ones which will be reproduced virtually.

Empirical methods are only successful when applied to seals that are very similar to those which were empirically studied. Numerical methods with computational fluid dynamics (CFD) are now used to predict seals performance. However most of the

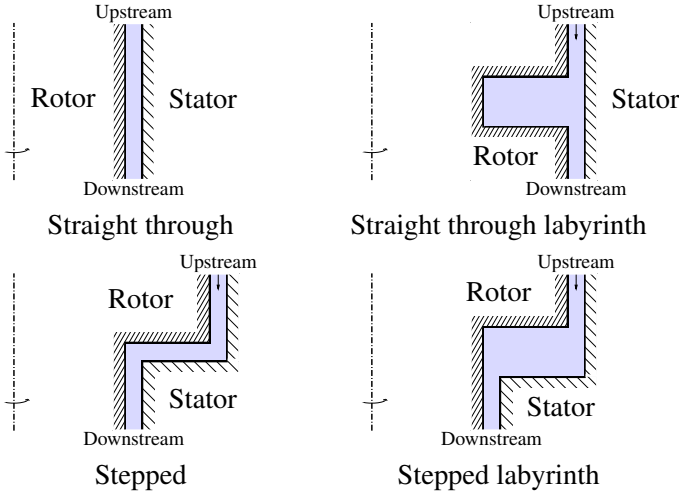


FIGURE 1. MOST COMMON HYDRAULIC SEALS GEOMETRIES

numerical studies of seals known to the authors deal with gas labyrinth seals and use the $k - \epsilon$ turbulence model: the labyrinth seals of gas turbines have been widely studied.

In the case of hydraulic seals, since the viscous losses in the boundary layer influence the leakage loss, the accurate computation of the flow in the boundary layer is of significant importance and low Reynolds turbulence models appear more appropriate [9, 10]. This paper presents a study that aims to implement an accurate CFD model to predict losses in hydraulic seals using a low Reynolds turbulence model and validate using experimental results for straight through labyrinth seals. The issues of the mesh, boundary conditions (pressure vs. flow rate boundary condition, estimate of the losses at the exit of the seal, etc.) are addressed. The commercial CFD code ANSYS CFX 12, which will be referred to as “Ansys” in this paper, is used.

This study focuses on straight-through labyrinth seals. Every tested geometry can be described with the parameters H , T , L , R and c , shown on Fig. 2. On this picture, the dimensions have been scaled for more clarity. Actual real-scale geometries can be seen on Fig. 4. Parameters H and T are respectively the height and thickness of the cavity, while L is the total length of the seal, R the radius of the rotor and c the seal clearance, also called gap.

One has to pay a particular attention here to which part is the rotor and which is the stator: in our geometries, the rotating part is the smooth one. This kind of seal is rightly called “tooth on stator”, or TOS [11]. Flows inside those seals are different from flows in “tooth on rotor” -or TOR- seals, which are more common on hydraulic turbines. As the only experimental data available to the authors was measured on TOS geometries, the CFD simulations will also be carried out using the same geometries.

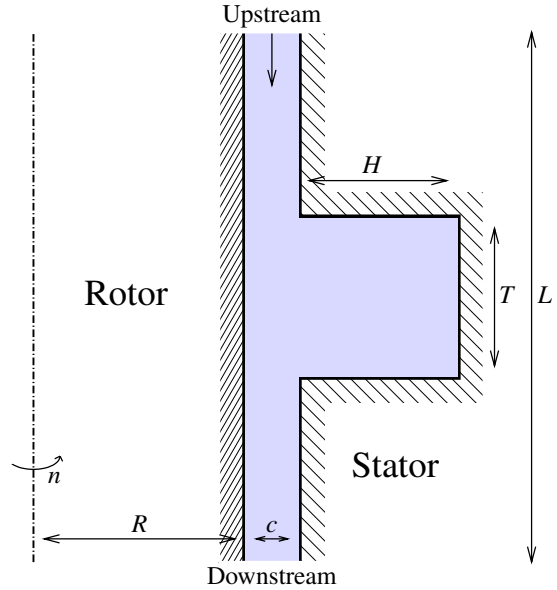


FIGURE 2. GEOMETRY OF THE TESTS

tries.

Of course, the geometric parameters are not the only ones in play. The flow also depends on:

1. The pressure drop between upstream and downstream ΔP .
2. The rotation speed of the rotor n .
3. The fluid properties: its density ρ and viscosity η .

There are two ways of considering the problem. On the one hand, when a flow rate is imposed to the seal, the result of the experience (or the result of the CFD simulation) is the pressure drop: that is what will be done during the simulations. And on the other hand, if a pressure drop is imposed, the result is the flow rate. That is what was done during the experimental investigation.

Choosing this second way, the problem can be summed up using the relation

$$Q = f(L, H, T, R, c, \eta, \rho, n) \quad (1)$$

The roughness of the walls can also be taken into account. To keep the problem simple, it will not be explicitly mentioned as a parameter.

Existing studies and models can accurately enough predict the behavior of straight seals [6, 9, 10], but the significance of the shape of the cavity is not well known. So one of the aims of this research is to determine the influence of the shape of the cavity of a straight-through labyrinth hydraulic seal on its performance.

Based on the results of this study, one can assume that CFD can be used to compute a surrogate model for hydraulic seals. This model has to use an appropriate design of experiments: in order to be accurate, it must use the results of points which are properly distributed across the design space. Such designs are known as “space-filling designs”. The final aim is to create a mathematical model, based on well-chosen numerical experiments, which would accurately enough predict the losses in a given seal. This way, other geometries could be studied, and their performances predicted. More particularly, the geometries which will be dealt with in the future are stepped labyrinths, which are widely used on high-head Francis turbines.

NOMENCLATURE

c	Seal clearance (or gap) [m]
$C_Q = \frac{Q}{c^2 \sqrt{\Delta P}}$	Discharge coefficient, dimensionless
ΔP	Pressure drop of the seal [Pa \equiv kg m ⁻¹ s ⁻²]
η	Dynamic viscosity of the fluid [kg m ⁻¹ s ⁻¹]
f	Outlet head loss coefficient, dimensionless
H	Height of the cavity [m]
k	Turbulent kinetic energy [m ² s ⁻²]
L	Total seal length [m]
n	Rotation speed [rad s ⁻¹]
ν	Kinematic viscosity of the fluid [m ² s ⁻¹]
ω	Turbulent frequency [s ⁻¹]
Q	Volumic flow rate through the seal [m ³ s ⁻¹]
R	Radius of the rotor [m]
$Re_\theta = \frac{\rho c n R}{\eta}$	Tangential Reynolds number, dimensionless
$Re_z = \frac{\rho c v_z}{\eta}$	Axial Reynolds number, dimensionless
ρ	Density of the fluid [kg m ⁻³]
T	Thickness of the cavity [m]
v	Total speed of the flow [m s ⁻¹]
v_n	Normal speed at the outlet [m s ⁻¹]
v_θ	Tangential speed of the flow [m s ⁻¹]
v_z	Axial speed of the flow [m s ⁻¹]

CFD MODEL

This part details the specifications of the CFD model which was chosen for our study. First, the choice of the SST turbulence model is justified. Meshing considerations are then explained, before addressing the issues of the boundary conditions.

The SST turbulence model

Our CFD model uses the low-Reynolds SST turbulence model for various reasons. As our study uses the commercial code Ansys, the simplest way to model turbulence is to choose among the built-in solutions. The SST model seemed the most

appropriate, because it uses both $k - \omega$ (for modelling the flow near the walls) and $k - \varepsilon$ behaviors (for higher Reynolds). Moreover, the wall roughness can be taken into account in the latest version of the code.

First, let us consider the steady-state incompressible isothermal Navier-Stokes equations which will be solved.

$$\rho \left(\frac{\partial \mathbf{U}}{\partial t} + \mathbf{U} \cdot \nabla \mathbf{U} \right) = -\nabla p + \mu \nabla^2 \mathbf{U} \quad (2)$$

$$\nabla \cdot (\rho \mathbf{U}) = 0 \quad (3)$$

Before understanding why the SST turbulence model is appropriate, let us sum up its specifications. As detailed in the help files of Ansys [12], its behavior is governed by the following equations.

Near the walls, the $k - \omega$ is used [12, 13]:

$$\frac{\partial (\rho k)}{\partial t} + \nabla \cdot (\rho \mathbf{U} k) = \nabla \cdot \left[\left(\mu + \frac{\mu_t}{\sigma_{k1}} \right) \nabla k \right] + P_k - \beta' \rho k \omega \quad (4)$$

$$\begin{aligned} \frac{\partial (\rho \omega)}{\partial t} + \nabla \cdot (\rho \mathbf{U} \omega) = \nabla \cdot \left[\left(\mu + \frac{\mu_t}{\sigma_{\omega 1}} \right) \nabla \omega \right] \\ + \alpha_1 \frac{\omega}{k} P_k - \beta_1 \rho \omega^2 \end{aligned} \quad (5)$$

On the other hand, further from the walls, $k - \varepsilon$ is used [12]:

$$\frac{\partial (\rho k)}{\partial t} + \nabla \cdot (\rho \mathbf{U} k) = \nabla \cdot \left[\left(\mu + \frac{\mu_t}{\sigma_{k2}} \right) \nabla k \right] + P_k - \beta' \rho k \omega \quad (6)$$

$$\begin{aligned} \frac{\partial (\rho \omega)}{\partial t} + \nabla \cdot (\rho \mathbf{U} \omega) = \nabla \cdot \left[\left(\mu + \frac{\mu_t}{\sigma_{\omega 2}} \right) \nabla \omega \right] \\ + 2\rho \frac{1}{\sigma_{\omega 2} \omega} \nabla k \nabla \omega \\ + \alpha_2 \frac{\omega}{k} P_k - \beta_2 \rho \omega^2 \end{aligned} \quad (7)$$

The transition between those two models in the upper boundary layer is done by using the following expression:

$$\Phi_3 = F \Phi_1 + (1 - F) \Phi_2 \quad (8)$$

Where Φ_1 , Φ_2 and Φ_3 respectively stand for the coefficients of the $k - \omega$ model, the $k - \varepsilon$ model, and the SST model, and F is the blending function, given by

$$F = \tanh \left(\max \left(\frac{2\sqrt{k}}{\beta\omega y}, \frac{500v}{y^2\omega} \right)^2 \right) \quad (9)$$

where y is the distance to the nearest wall.

Moreover, the SST model also uses a limiter to the eddy viscosity:

$$v_t = \frac{\mu_t}{\rho} = \frac{a_1 k}{\max(a_1 \omega, SF_2)} \quad (10)$$

In all those equations, β' , α_1 , α_2 , β_1 , β_2 , $\sigma_{\omega 1}$, $\sigma_{\omega 2}$, σ_{k1} , σ_{k2} are constants of the model (cf. [12, 13] for details and numerical values), while P_k is the turbulent energy production, given by

$$P_k = \mu_t \nabla \mathbf{U} \cdot (\nabla \mathbf{U} + \nabla \mathbf{U}^T) - \frac{2}{3} \nabla \cdot \mathbf{U} (3\mu_t \nabla \cdot \mathbf{U} + \rho k) \quad (11)$$

Viscous forces and scale issue. When looking at a hydraulic seal, one has to remember the context of the study. The seal is a tiny gap between the rotor and the stator. So tiny that given the Reynolds number we are dealing with (typically below a few tens of thousands), boundary layer flows can be significant, and their influence on the main flow non-neglectible. That is why modeling the flow near the wall is crucial, and why a $k - \omega$ turbulence model would be interesting.

Wall roughness. To be as accurate as possible, our turbulence model should take into account the effect of roughness when it models the flow near the wall [9]. But paradoxically, the model using smooth walls has given better results. That is why the walls were considered smooth for our simulations.

Meshing considerations

Axisymmetric hypothesis. The main geometric hypothesis which was made is that the flow is axisymmetric, meaning no 3D effect will be taken into account. This hypothesis can be made after having had a look at Fig. 3, which represents the domains where vortices can appear. It was used in previous studies [5, 10]. The tests which were chosen for validating the model are summed up in Tab. 4. As none of them are in the “vortices” domain because axial Reynolds numbers Re_z are too high, one can assume there will be no 3D effect.

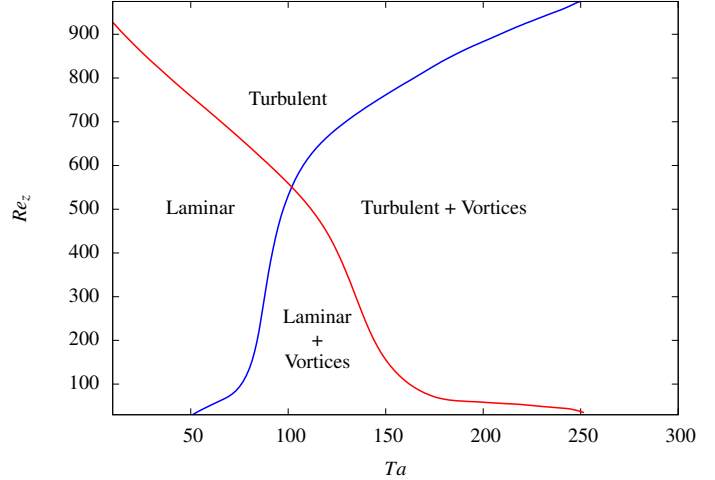


FIGURE 3. FLOW REGIMES

General mesh characteristics. The mesh which was used is a structured 2D-like mesh. As Ansys is not able to perform directly 2D simulations, a 2D mesh was extruded by rotation, forming a 3D one layer-thick mesh which can be used by the solver. This solution was advised by the Ansys documentation and remarks from previous studies [9, 10]. The angular amplitude of the extrusion was chosen willingly small, so that thin elements do not degenerate.

Parabolic distribution. As our SST turbulence model necessitates enough nodes near the wall to compute properly the boundary layer flow, a parabolic distribution of the nodes was used. This way, enough nodes are located along the walls of the cavity and along the walls of the upstream and downstream straight seals. Moreover, the parabolic distribution was used in previous studies [9, 10] and has proven efficient. An example of a coarse mesh (used for test number 1919) is shown on Fig. 4.

First node. Once again, to compute properly the near-wall flow, the first node has to be really close to the wall. The $y^+ < 2$ criteria, advised by Wilcox [13] and the Ansys help [12] has to be respected. So one of the important parameters of the mesh is the distance between the wall and the first node, which is set to $0.001c$ (a thousandth of the seal clearance).

Boundary conditions

Inlet. Two types of inlet boundary conditions were used. The first and most obvious one is the uniform normal speed, which was used for “non-rotating” tests. If this boundary condition is used when the rotor moves, a discontinuity is created: near the rotor, the movement is purely tangential, whereas the

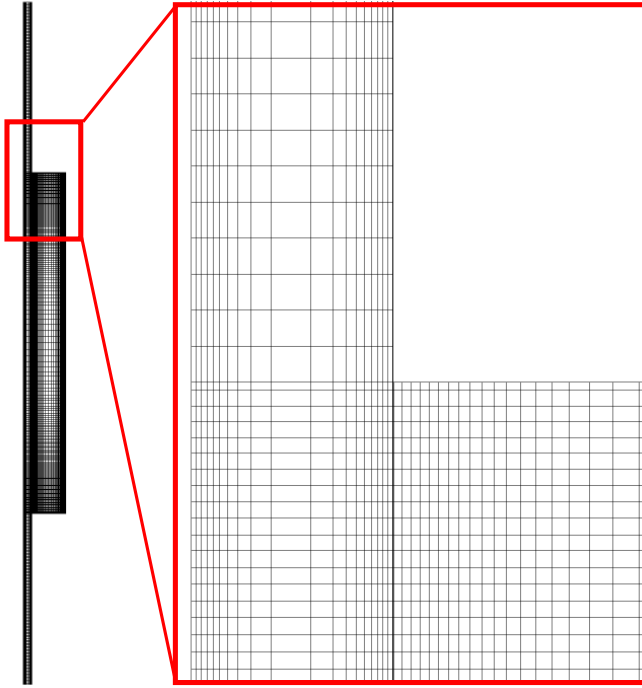


FIGURE 4. MESH EXAMPLE

TABLE 1. MODEL AND PROTOTYPES DIMENSIONS

	c [mm]	R [m]	$\frac{R}{c}$
Model	0.3 to 2.54	0.2286	90 to 600
Prototype	~ 0.5	~ 2.5	~ 5000

Computing considerations

Two different setups were used to perform the computations. The first and most efficient one is a Dual-quadcore, 24GB RAM computer. The second one is a LAN cluster of two to six workstation otherwise idle during nighttime. For a given geometry, the result of each grid refinement was used as initial conditions for the next one, in order to accelerate the convergence. CFX-Solver's timescale factor was also modified depending on the behavior of each test, once again to improve the convergence speed.

EXPERIMENTAL DATA

Test results

In the sixties, straight through labyrinth seals have been studied by Dominion Engineering Works. All geometries are similar to the one described on Fig. 2, with variations of the various geometric parameters. Even if the experiment had not been designed with the intent of constructing a numerical model, many tests are useable for our study.

Each geometry has been tested on various operation points. For each operation point, two significant values were measured:

1. The pressure drop between upstream and downstream, H , in feet of water.
2. The flow rate through the seal, Q , in cubic feet per second.

Outlet pressure (symbolized H'') was also recorded. As our study does not deal with cavitation, this measure will not be taken into account.

Range of the tests

The experimental apparatus used to study the seals is quite different from the actual turbines. The most important difference is that the gap is much thinner on turbine prototypes than on the models, as details Tab. 1. As this study aims particularly at taking into account the effect of the cavity of the seal, $\frac{R}{c}$ is not the most important factor. But this true difference between simulated and experimented geometries and the actual turbines has to be kept in mind.

Data treatment

In order to simplify and generalize the problem, the experimental data was nondimensionalized. This process is detailed

imposed speed on the inlet is purely axial. That is why imposing fully developed flow profiles is a better solution for " $n \neq 0$ " tests, the main drawback being in this case the additional computation of the profiles.

Another option, which was not really used, is to set the inlet pressure. But, as it was reported in V. Le Roy's Masters Thesis [9], and as it was observed when running the tests, that convergence was slower when using such boundary conditions.

Outlet. Two different boundary conditions have been tested. The first and most simple one imposes an average static pressure. The other one is called "Opening" in Ansys. It allows the computation of a head loss at the outlet of the seal, which is based on the normal speed at the outlet. The direction of the flow can be automatically computed, and the head loss $\frac{1}{2}\rho f v_n^2$ can be adjusted by the user, who has to enter the f coefficient. Moreover, there are no details in the Ansys help [12] about what truly happens when one chooses this boundary condition. As detailed below, its use has been abandoned after a few tests, because it slowed convergence and did not give truly better results than the average pressure condition.

below.

Inputs of the problem. Before making the data dimensionless, one has to look at the various inputs of the problem. They can be listed as follows:

1. Geometric parameters: the seal length L , the height and length of the cavity H and T , the rotor radius R and the seal clearance c , all in meters.
2. Fluid-related parameters: its density ρ , in kg m^{-3} and dynamic viscosity η , in $\text{kg m}^{-1} \text{s}^{-1}$.
3. The pressure drop, ΔP , in mH_2O or Pa.
4. The flow rate through the seal, Q , in $\text{m}^3 \text{s}^{-1}$.
5. The rotation speed of the rotor, n , in rad s^{-1} .

As written earlier, the wall roughness is also a parameter of the problem. But its influence being relatively limited, it will be deliberately omitted here, until the CFD simulations are dealt with.

Nondimensionalization. In order to nondimensionalize the data, the Buckingham Π theorem was used. There are 10 parameters and 3 units. So the problem can be described using only 7 dimensionless parameters.

If the reference values are c , ρ and ΔP , the problem can be expressed nondimensionally in the following way.

$$C_Q = f\left(\frac{L}{c}, \frac{H}{c}, \frac{T}{c}, \frac{R}{c}, \frac{1}{\sqrt{Eu_\theta}}, \frac{1}{Re}\right) \quad (12)$$

With:

1. C_Q a discharge coefficient defined by $C_Q = \frac{Q}{c^2 \sqrt{\frac{\Delta P}{\rho}}}$.
2. $\frac{1}{Re}$ the inverse of a Reynolds number given by $Re = \frac{c \sqrt{\frac{\Delta P}{\rho}}}{\eta}$.
3. $\frac{1}{\sqrt{Eu_\theta}}$, with Eu_θ the tangential Euler number: $Eu_\theta = \frac{\Delta P}{(nc)^2 \rho}$.

These parameters, which are the direct results of the nondimensionalization using Buckingham's theorem, are not the most easy to interpret. That is why the more common axial and tangential Reynolds numbers, $Re_z = \frac{\rho c v_z}{\eta}$ and $Re_\theta = \frac{\rho c n R}{\eta}$, will also be used to identify the tests.

Uncertainties

Experimental values. All the experimental uncertainties on dimensional parameters are summed up in Tab. 2. This table contains averaged values on the whole set of tests. One has to pay attention to the fact that depending on the test, the relative uncertainty on geometric parameters, and on the gap c in particular, varies. For example, if the uncertainty on the gap value is

TABLE 2. UNCERTAINTIES ON THE EXPERIMENTAL DATA

Variable	Absolute uncertainty	Mean relative uncertainty
c	± 0.001 in	2.4 %
R	± 0.001 in	0.0 %
T	± 0.001 in	0.2 %
H	± 0.002 in	1.0 %
L	± 0.005 in	0.1 %
n	± 2 rpm	0.2 %
v	n.a.	4.8 %
ρ	n.a.	0.0 %
ΔP	n.a.	1.0 %
Q	n.a.	1.5 %

0.001 in, a 0.1 inch-wide gap will have a 1 % uncertainty, while the uncertainty on a 0.01 inch-wide gap would be 10 %. That is why thin-gap tests will have higher uncertainties.

One of the most uncertain parameters is not listed explicitly in Tab. 2 but plays an important role: the temperature of the water. It is not specified in the report, so it was assumed to be equal to 21 °C, based on other tests on straight seals [8]. One has to pay a particular attention to this hypothesis, as a variation of 5 °C provokes a variation of about 12 % of the viscosity of the water. In order to maintain uncertainties below reasonable values, a variation of ± 1 °C around 21 °C was assumed, and empirical formulas were used to compute uncertainties on the viscosity and density of the fluid.

Nondimensional parameters. Dimensional experimental uncertainties lead to uncertainties on dimensionless variables. Table 3 sums up the tolerances of the nondimensionalized parameters. Once again, those mean values were obtained by averaging over the whole set of tests, and the actual values vary depending on the test.

One can remark that uncertainties on dimensionless variables are higher. That is because each nondimensionalized parameter accumulates the uncertainties from the corresponding dimensional values. The mean values of the table were calculated on the entire set of tests. The most important value to keep in mind is the uncertainty on the discharge coefficient, because it is the variable upon which the comparison between experience and CFD simulations is based.

TABLE 3. UNCERTAINTIES ON NONDIMENSIONALIZED VARIABLES

Variable	Mean relative uncertainty
$\frac{R}{c}$	2.4 %
$\frac{T}{c}$	2.6 %
$\frac{H}{c}$	3.3 %
$\frac{L}{c}$	2.5 %
$\frac{1}{Re}$	8.6 %
$\frac{1}{\sqrt{Eu_\theta}}$	2.8 %
C_Q	6.5 %

Eccentricity. In this study, the rotating and non-rotating parts have been considered purely concentric. No eccentricity effect has been considered. Actually, the experimental eccentricity and dynamic effects, which can not be exactly zero, can induce an additional uncertainty, which was not taken into account.

MODEL VALIDATION

Chosen tests

The geometric parameters, and the specifications of the operation points of the cases which were run are summed up in Tab. 4. In the end, six geometries were numerically simulated, and for each geometry, four operation points were run.







Model verification procedure

Our CFD model is verified using a sequence of resolution and mesh refinement steps, according to the following procedure. First, a coarse mesh is generated. The case is then set up in the preprocessor, using the parameters and boundary conditions which were chosen for the test. Once the run is ready, it is solved using CFX. The solver is set so that the convergence be as tight as possible (RMS residuals below 10^{-6}), this way, the iteration error is minimal. The process is then iterated several times (ten times in most cases) for each test, with the grid being refined by a $\sqrt{2}$ factor at each step.

The whole process has been automated using awk scripts as follows.

1. Initialization.
2. For each test:
 - (a) Read input data.
 - (b) Initialize run.
 - (c) Compute the successive refinements.

TABLE 4. CHOSEN TESTS

Test number	Geometry	Re_z	Re_θ	Ta	
1919		$\frac{R}{c} = 90$	47786	0	0
		$\frac{L}{c} = 80$	46488	37241	3926
		$\frac{H}{c} = 4$	58361	74485	7851
		$\frac{T}{c} = 40$	13142	74485	7851
1879		$\frac{R}{c} = 120$	41900	0	0
		$\frac{L}{c} = 63.3$	60256	27932	2550
		$\frac{H}{c} = 5.7$	40874	55864	5100
		$\frac{T}{c} = 10$	20326	55864	5100
1852		$\frac{R}{c} = 120$	31979	0	0
		$\frac{L}{c} = 63.3$	39747	27932	2550
		$\frac{H}{c} = 10.7$	30389	55864	5100
		$\frac{T}{c} = 10$	11270	55864	5100
1814		$\frac{R}{c} = 180$	21251	0	0
		$\frac{L}{c} = 90$	37634	18621	1388
		$\frac{H}{c} = 16.5$	12095	37242	2776
		$\frac{T}{c} = 10$	33165	37242	2776
1819		$\frac{R}{c} = 180$	31999	0	0
		$\frac{L}{c} = 110$	15858	18621	1388
		$\frac{H}{c} = 16.5$	18475	37242	2776
		$\frac{T}{c} = 30$	7164	18621	1388
1805		$\frac{R}{c} = 360$	10566	0	0
		$\frac{L}{c} = 200$	7986	9311	491
		$\frac{H}{c} = 4$	9449	18621	981
		$\frac{T}{c} = 40$	3989	18621	981

- (d) Create the global results file and asymptotic convergence graph.

In the end, about ten gradually refined results are produced for each operation point. They are then extrapolated using Richardson's extrapolation to get an evaluation of the asymptotic value of the predicted flow discharge coefficient C_Q .

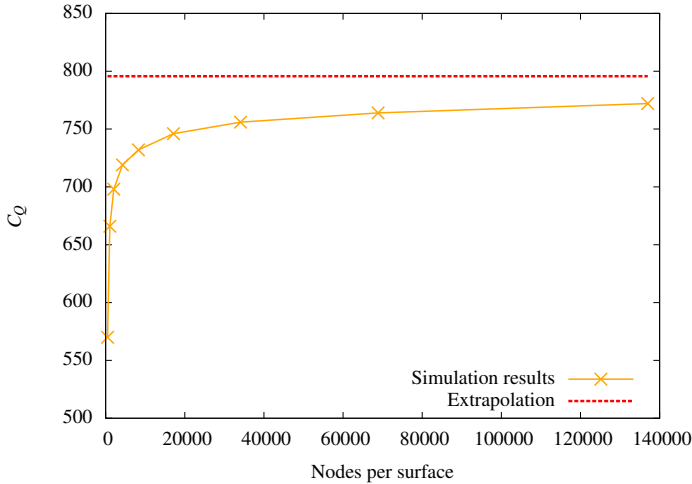


FIGURE 5. EXAMPLE OF ASYMPTOTIC CONVERGENCE

Results

Asymptotic convergence. For each test (given geometry, given working conditions), the mesh refinement study leads to a graph similar to the one reproduced on Fig. 5. The x axis is the number of 2D nodes (remember, CFX does not perform 2D simulations, so the actual mesh contains twice as many nodes), and the ordinate is the value of the discharge coefficient C_Q . C_Q was chosen to monitor the asymptotic convergence for two reasons. The first and most obvious is that it is the variable used to compare the simulations to empirical results. And second, C_Q is a global rather than pointwise quantity: it thus reflects the behavior of the whole system.

Outlet headlosses. For each test, three discharge coefficients were computed, using respectively:

1. The pressure drop of the seal, ie. the difference between the inlet and the outlet sections.
2. The pressure drop plus a headloss, given by $\frac{1}{2}\rho f v_n^2$ (normal-speed-based correction) or $\frac{1}{2}\rho f v^2$ (total-speed-based correction). As the *average static pressure* boundary condition has been used, the headloss has been computed *a posteriori*.

The correction accounts for the headlosses due to the sudden expansion at the outlet of the seal. The f coefficient was set to 1, following the recommendations of previous studies [9, 11]. This seems to be a valid hypothesis, as the results of our model are not far from the empirical values.

As can be seen on Fig. 6, the difference between corrected values and “no headlosses” values is significant.

No inlet correction was considered, as previous studies have shown that they were not significant compared to the outlet losses [9].

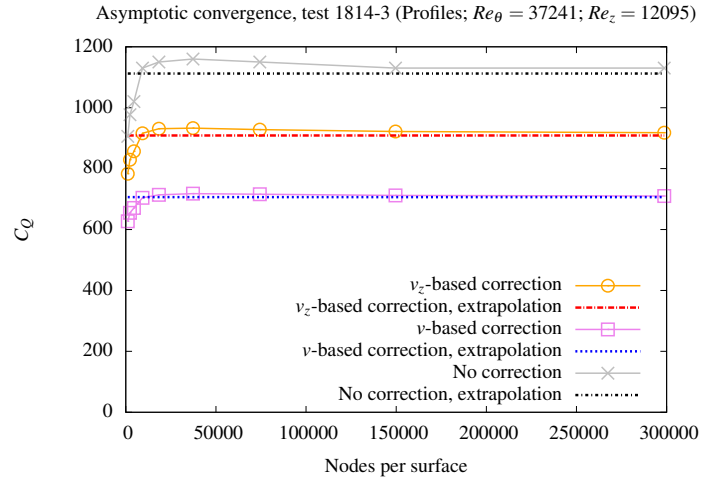


FIGURE 6. OUTLET HEADLOSSES

TABLE 5. STATISTICS OF THE DISCREPANCY

	Minimum	Maximum	Average	RSD
Discrepancy	0.13 %	17.81 %	6.49 %	75.60 %

Comparison between CFD and experimental results. A few comments can be made about the results:

1. In general, the discrepancy between CFD results and empirical values is relatively low.
2. More than 61% of the discrepancies are below the uncertainty of the experience.
3. Some tests seem more accurate than others: for example, the discrepancies for geometry number 1805 are significantly worse. Sadly, there is no obvious reason why some of the CFD results are closer to the experiments, while others do not fit well.

As summed up in Tab. 5, depending on the test, the error varies from 0.13 % to 17.81%, the mean value being below 7 %. The relative standard deviation is quite high, meaning this mean value can not be considered accurate for each test.

CONCLUSIONS AND FURTHER WORK

The results of this study can be summed up as follows. Given significant hypotheses:

1. Steady-state, incompressible, isothermal flow conditions.
2. Outlet headlosses based on the normal speed.
3. No eccentricity.

The following assumptions can be made.

1. The CFD model using SST turbulence modeling, parabolic mesh distributions, speed-based inlet boundary conditions, pressure-based outlet boundary conditions and an outlet headloss correction based on the normal speed can reproduce with an acceptable precision the experimental results of the tests which were chosen.
2. This model gives relatively accurate macroscopic predictions of the discharge coefficient C_Q , but nothing can be assumed on internal flow conditions and turbulence modelling.

The results of this study are highly linked to the geometries which were studied. As there is no experimental data for hydraulic seals of actual turbines, this model has not been validated in these actual cases: further research has to be lead in this field.

Flows in stepped labyrinth seals could be studied using the model presented in this study, but the further results will have to be taken with extreme caution, as no empirical data is available. The next step of our research involves using a computer-simulations-specific design of experiments to create a surrogate model of those seals using cautiously the model described in this paper. The surrogate model will have to be accurate enough to be used by semi-empirical methods. The study of stepped labyrinth geometries has been chosen because they are used on high head turbines, for which the losses in the hydraulic seals are particularly high. Using a surrogate model combined with semi-empirical methods, a geometric optimization is to be performed in order to increase the efficiency of those turbines.

ACKNOWLEDGMENT

Special thanks to the Natural Sciences and Engineering Research Council of Canada and Andritz Hydro Limited, who finance this research, and to Andritz Hydro Limited for granting us access to their experimental data.

REFERENCES

- [1] Sneck, H. J., 1974. "Labyrinth seal literature survey". *Journal of Lubrication Technology*, **96**, pp. 579–582.
- [2] Ng, C. W., and Pan, C. H. T., 1965. "A linearized turbulent lubrication theory". *ASME Journal of Basic Engineering*, **87**, pp. 675–688.
- [3] Elrod, H., and Ng, C. W., 1967. "A theory of turbulent films and its application to bearings". *ASME Journal of Lubrication Technology*, **89**, pp. 347–362.
- [4] Lang, J., 1964. Investigation of discharge coefficient for different labyrinth seals. Tech. Rep. 53-1356-BT, Dominion Engineering Works, Ltd.
- [5] Vu, T., 1976. Analysis of straight seal tests. Tech. Rep. 1230-7, Dominion Engineering Works Ltd.
- [6] Vu, T., 1978. Straight seal analysis and computer program. Tech. Rep. 1230-17, Dominion Engineering Works Ltd.
- [7] Vu, T., 1978. Viscous seal : theoretical analysis and computer program. Tech. Rep. 1230-18, Dominion Engineering Works Ltd.
- [8] Akgungor, A., and Vu, T. C., 1974. Experiments on 2.5" straight sleeve seals. Tech. Rep. 1205-6, Dominion Engineering Works, Ltd., Lachine, Québec.
- [9] Roy, V. L., 2008. Étude numérique et semi-empirique de joints hydrauliques d'étanchéité droits et escalier.
- [10] Roy, V. L., Guibault, F., and Vu, T., 2009. "Validation of a CFD model for hydraulic seals". *International Journal of Fluid Machinery and Systems*, **2**(4), pp. 400–408.
- [11] Rhode, D., and Nail, G., 1992. "Computation of cavity by cavity flow development in generic labyrinth seals". *Journal of Tribology*, **114**, pp. 47–51.
- [12] ANSYS Inc., 2009. *ANSYS CFX-Solver Theory Guide*.
- [13] Wilcox, D. C., 1993. *Turbulence Modeling for CFD*.